American Mineralogist, Volume 91, pages 511–516, 2006

Vacancy defects in MgO at high pressure

BIJAYA B. KARKI* AND GAURAV KHANDUJA

Department of Computer Science, Louisiana State University, Baton Rouge, Louisiana 70803, U.S.A.

ABSTRACT

First-principles calculations within the local density and pseudopotential approximations were performed to investigate the effects of pressure on the energetics and structural behavior of charged vacancy defects in MgO. The simulations were performed for a supercell containing 216 atoms with their positions being fully optimized. In particular, the formation and migration energies of cation and anion vacancies were shown to substantially increase over the pressure regime of the Earth's mantle. Our results thus suggest that pressure should suppress intrinsic diffusion mediated by ionic vacancies in MgO over the mantle pressure regime. The calculated three-dimensional data sets for atomic displacements and electron charge density were explored in detail using an interactive visualization system. Although the atomic and electronic structures are highly distorted in the close vicinity of the defects (i.e., in the region covering up to the nearest and next-nearest atoms), the effects are not negligible at farther distances.

Keywords: Defects, mantle minerals, high pressure, rheology, first-principles calculations, scientific visualization

INTRODUCTION

Point defects such as cation and anion vacancies in MgO have been subject of extensive theoretical (e.g., Sangster and Rowell 1981; De Vita et al. 1992a, 1992b; Gibson et al. 1994; Vocaldo et al. 1995; Ita and Cohen 1997, 1998; Scorza et al. 1997; Alfe and Gillan 2005) and experimental (e.g., Duclot and Departes 1980; Sempolinski and Kingery 1980; Yang and Flynn 1994) investigations because of its importance as a prototype oxide and major mantle component. Studies of point defects in silicate minerals are also common (e.g., Wright and Catlow 1994; Brodholt 1997; Watson et al. 2000; Walker et al. 2003). A detailed knowledge about the defect energetics and structural properties, particularly at high pressure, is critical to our understanding of mantle rheology because defects control diffusion and creep processes in minerals. The distorted crystal lattice around defects provides rapid diffusion pathways within crystals. As such, the dominant diffusion mechanism may be vacancy hopping and even the dominant deformation mechanism may be diffusion creep or diffusion-controlled dislocation climb.

First-principles studies of point defects in solids have been increasingly common in recent years due to the possibility of simulating systems involving several tens to several hundreds of atoms (e.g., De Vita et al. 1992a; Brodholt 1997; Ogut and Chelikowsky 2001; Lento et al. 2002; Alfe and Gillan 2005). To obtain accurate results for the defect energetics and understand the related atomic and electronic structures in detail require simulation of a large atomic system, which is now becoming feasible. More importantly, previous first-principles calculations were performed only at zero pressure although the simplified empirical molecular dynamics (Mills et al. 1991) and non-empirical variational-induced breathing model approaches were previously performed at high pressures and temperatures (Ita and Cohen 1997, 1998). Since MgO is thought to be the second most abundant mineral of the Earth's lower mantle, occurring in the form of magnesowusite, (Mg,Fe)O, it is essential to more accurately characterize its defect properties at realistic conditions of the Earth's deep interior.

In this paper, we report first-principles quantum-mechanical investigations of two charged vacancies (Schottky pair) in MgO at geophysically relevant pressures using a combination of computational and visualization techniques. A well-established super cell method involving a few hundred atoms was used to calculate the defect-related properties including formation and migration energies as a function of pressure. The resulting three-dimensional data sets were also successfully visualized to gain insight onto the atomic and electronic structures of the defects.

METHODOLOGY

Computational technique

Calculations were performed using the parallel code PWscf (Plane-Wave Self-Consistent Field), which is based on density functional theory within the local density approximation (Baroni et al. 1987; Giannozzi et al. 1991; www.pwscf.org). The Mg and O pseudopotentials were the same as those, which were successfully used in our previous calculations involving MgO (see Karki et al. 2000). A plane wave basis set with cutoff of 70 Ry was used to expand the valence electronic wave function. Brillouin Zone summations of electronic quantities were performed over four special k-points for the equilibrium structure, and higher numbers of equivalent points up to 12 points for the defective lattice with migrating ion (Monkhorst and Pack 1976). The energy differences were found to converge to better than 0.02 eV.

A super cell of MgO containing 216 atoms was used. The effect of system size was also explored by simulating smaller super cells with 32 and 64 atoms. A defective super cell contained only one charged defect of given type at a time. A cation vacancy was created by removing an Mg core, leaving two valence electrons in the system, while an anion vacancy was formed by removing an O core together with eight valence electrons. Thus, the net charges of the Mg and O vacancies, which are known as V^{2-} and F^{2+} centers, were –2e and 2e, respectively. The ionic

* E-mail: karki@bit.csc.lsu.edu

vacancies in MgO can have other states such as neutral and singly charged states (see Gibson et al. 1994). However, here we only study these doubly charged vacancies, which form Schottky pairs, the dominant point defects in MgO. Due to a net defect charge associated with the super cell, two treatments were needed to obtain acceptable results. The first was to use the Ewald sum for the long-range coulombic interactions by assuming that there is a counter-charge distributed uniformly throughout the simulation cell (Leslie and Gillan 1985). The second was to make an appropriate correction for defect-defect interactions arising from a periodic array of defective cells because we were interested in the energy of an infinite lattice containing only one charged defect. The defect-defect correction whose magnitude decreases with the size of the supercell was made using (Leslie and Gillan 1985; also see Lento et al. 2002)

$$\Delta E = -\frac{\alpha q^2}{2\varepsilon L}$$

where q is the charge of the defect and α is the appropriately defined Madelung constant for a supercell of length L. This expression simply represents the electrostatic energy of an array of point charges in a neutralizing background in the presence of a screening medium described by the static dielectric constant ε. The values of α are 2.837, 2.888, and 2.885 for SC, BCC and FCC supercells, respectively (Lento et al. 2002). The required value of ε as a function of pressure was taken from the first-principles lattice dynamics calculations (Karki et al. 2000).

We used a constant-volume approach to simulate a defective MgO system (Wright and Price 1993; Ogut and Chelikowsky 2001; Alfe and Gillan 2005). The other common approach was based on constant pressure (Mills et al. 1991; Watson et al. 2000; Mukherjee et al. 2003). In the constant-volume approach used here, the pressure-volume relationship for the perfect crystal was first obtained by fitting a fourth-order finite strain equation to the calculated energy-volume data. Defect calculations were then performed as a function of pressure using corresponding volumes. At each pressure, the volume of a given defective system was kept fixed at the corresponding perfect lattice volume so only the internal energy was of concern in the calculation of defect energetics. We showed that the constant-volume approach essentially produces energetics similar to the constant-pressure approach, in which enthalpy is of concern (Table 1). We also found that the two approaches yield similar atomic and electronic structures for 216 atoms per cell although the structural differences are larger for smaller cells. This is consistent with the fact that the ratio between defective (V_D) and perfect (V_P) volumes deviates less from unity as the cell size increases. For Mg-vacancy systems, V_D/V_P is 1.019, 1.013, and 1.004, respectively, for cell sizes of 32, 64, and 216 atoms, whereas for O-vacancy systems the corresponding numbers are 0.968, 0.979, and 0.994. In other words, due to a relatively small supercell size, the defect concentration of the simulated system turns out to be relatively high (e.g., 1.56% defect in a 64 atom system), and the coupling between defect and lattice strain often results in a large volume change. However, our calculations were meant for a single defect in an infinite system for which the ratio V_D/V_P becomes one. The constant-volume approach thus avoids any unwanted contributions associated with such volume change of the finite super cell used in the simulation.

Visualization technique

Simulations that involve as many as 216 atoms and 864 electrons produce massive three-dimensional data sets for atomic configuration and charge density distribution. Here we exploit the visualization approach, which has, in recent years, emerged as an attractive approach to uncover important, otherwise hidden, information in large-scale sets of scientific data (e.g., Schroeder et al. 1997). Several visualization systems such as XCRYSDEN (Kokaji 1999, 2003), VMD (Humphrey et al. 1996), and Atomsviewer (Sharma et al. 2003) are available; however, using them is always not the best choice. First, these visualization packages are often not available for free download. Second, even if they are available, they do not have all options that one might need to successfully visualize a particular data set. Keeping in the mind the scenario that many more simulations of defective systems (involving point as well as extended defects) are yet to be performed, it is important to develop a visualization system that will be flexible enough and interactive enough to meet our specific needs. Such visualization development is currently under progress (Khanduja and Karki 2005). However, here we present relevant visualization outputs for the simulated geometric and electronic structures of defective MgO systems.

TABLE 1. Comparison between constant-volume (CV) and constant-pressure (CP) approaches for defect calculations performed at 100 GPa

	Internal Energy (E) (eV)	Volume (Å^3)	ΔE	$P\Delta V$	Extraction Energy (eV)
Perfect crystal:	–50336.463	1460.75			
Mg-vacancy: CV	–50280.724	1460.75	55.739	0	55.739
CP	–50284.412	1466.41	52.051	3.533	55.584
O-Vacancy: CV	–49919.722	1460.75	416.741	0	416.741
CP	–49914.368	1451.86	422.095	–5.549	416.546

Note: Extraction (formation) energies for Mg and O-vacancy defects are shown.

RESULTS AND DISCUSSION

Defect energetics

We calculated the cation and anion vacancy energies, that is, the energies required to extract an Mg^{2+} ion and an O^{2-} ion to form corresponding isolated ions. This involved subtracting the energy of each defective crystal from that of the perfect crystal and then subtracting the correction for the defect-defect interaction to obtain a more accurate result:

$$E_{Mg} = E_N(1,0) - E_N(0,0)$$
$$E_O = E_N(0,1) - E_N(0,0)$$

Here $E_N(0,0)$ is the relaxed total energy of the perfect crystal containing N lattice sites and whereas $E_N(1,0)$ and $E_N(0,1)$ both refer to systems in which the supercell has a net charge (–2e and 2e, respectively). The Schottky formation energy (E_S), which is simply the sum of the Mg^{2+} and O^{2-} vacancy energies minus the cohesive energy per ionic pair, was calculated using

$$E_S = E_N(1,0) + E_N(0,1) - [2(N-1)/N]\, E_N(0,0) = E_{Mg} + E_O + E_{pair}(0,0)$$

Here $E_{pair}(0,0)$ also includes the pressure-volume term at a given pressure. To calculate the migration energy of a given type of vacancy defect, we removed the corresponding ion from two nearest neighboring sites and then constrained one of the removed ions to lie halfway between the sites. In other words, the migrating ion was positioned at the middle of the line joining two neighboring half-vacancies. The resulting energy was subtracted from the energy of the corresponding equilibrium vacancy system. The migration energies are not affected by defect-defect correction since the same correction applies to both equilibrium and migrating vacancy systems. The calculated defect formation and migration energies are shown in Table 2. Our results compare favorably with previous calculations (Sangster and Rowell 1981; De Vita et al. 1992a; Ita and Cohen 1998; Walker et al. 2003; Alfe and Gillan 2005) and experiments (Mackrodt 1982; Duclot and Departes 1980; Sempolinski and Kingery 1980; Shirasaki and Hama 1973; Shirasaki and Yamamura 1970), as shown in Table 3.

The effects of ionic relaxation and system size of the defect systems were also explored in detail. The relaxation energies are substantial (Table 2). There are many more degrees of freedom for the 216-site (i.e., 216 atom) system compared to the 32-site system that was previously studied (De Vita et al. 1992a). All the degrees of freedom were fully relaxed. In the case of the migrating ions, all degrees of freedom other than the position of

TABLE 2. Calculated defect energetics (expressed in the units of eV) in MgO from total-energy calculations performed for Mg^{2+} and O^{2-} vacancies in 32-, 64-, and 216-site systems

	32 atoms	64 atoms	216 atoms
E_{pair}	–466.389	–467.282	–467.281
E_{Mg}: Unrelaxed	50.369	50.621	51.852
Relaxed	48.489	48.791	49.304
Corrected	49.815	49.780	49.964
E_O: Unrelaxed	424.390	432.357	426.090
Relaxed	423.007	423.560	423.486
Corrected	424.333	424.549	424.146
Schottky energy (E_S):			
Unrelaxed	8.370	8.927	10.662
Relaxed	5.107	5.070	5.509
Corrected	7.759	7.048	6.829
Migration energy:			
Mg vacancy	2.242	2.253	2.262
O Vacancy	2.374	2.410	2.424

Notes: The effects of ionic relaxations (Unrelaxed and Relaxed) and defect-defect interactions (Corrected) were explicitly taken into account. E_{pair} is the lattice energy per unit cell. E_{Mg} and E_O are Mg and O extraction energies, respectively. See the text for the definition of different energy terms used.

TABLE 3. Comparison of the calculated defect formation and migration energies (expressed in eV) with previous calculations: LDA (De Vita et al. 1992a), QMC (Alfe and Gillan 2005), MD (Sangster and Rowell 1981) and available experimental data for Schottky energy (Mackrodt 1982), migrating Mg vacancy energy (Duclot and Departes 1980; Sempolinski and Kingery 1980), and migrating O vacancy energy (Shirasaki and Hama 1973; Shirasaki and Yamamura 1970)

	This study (216 atoms)	LDA (32 atoms)	QMC (1000 atoms)	MD	Expt.
Schottky energy	6.829	6.884	6.76	7.72	4–7
Mg vacancy migration	2.262	2.393		2.07	2.20, 2.28
O vacancy migration	2.424	2.481		2.11	2.42, 2.61

the migrating ion itself were optimized. Our calculations show that the results are very similar for all the 32, 64, and 216 site systems (Table 2). The magnitude of defect-defect correction is smaller for a larger system but the corrected energies were found to be very similar for all system sizes. The present result also agrees well with recent calculation involving 1000 atoms (Alfe and Gillan 2005). This clearly implies that both the vacancy formation energies with appropriate correction for defect-defect interactions included and migration energies indeed converge rapidly with system size and even a few tens to a couple hundred atoms appear to be sufficient to obtain defect energetics with an acceptable accuracy.

The defect energetics were investigated as a function of pressure from –10 to 150 GPa as shown in Figure 1. The calculations show that both formation and migration energies are strongly dependent on pressure. With increasing pressure, their magnitudes increase relatively rapidly in the beginning and then more gradually at higher pressures. The values of Schottky formation energy and Mg and O vacancy migration energies at a negative pressure of 10 GPa differ from those at zero pressure by 22%, 15%, and 16%, respectively.

Atomic structure

The atoms surrounding a given vacancy site are expected to displace from their original positions in the perfect lattice. Unlike in previous studies, the simulation of relatively large 216-site systems allows us to analyze the atomic displacement field induced by the defect. The atomic structures of the fully

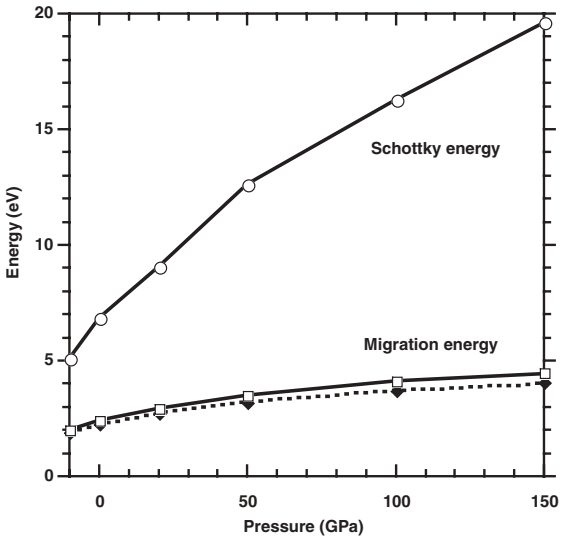

FIGURE 1. Pressure dependence of the Schottky formation energy (circles) and Mg^{2+} (squares) and O^{2-} (diamonds) vacancy migration energies. The errors are within the sizes of the symbols used.

relaxed vacancy systems were visualized by rendering atoms and their displacement vectors. A given vacancy site can be viewed as being surrounded by several atomic shells; for example, the first three shells contain the nearest (N), next nearest (NN), and next-next-nearest (NNN) neighbor atoms, respectively (Fig. 2a). Note that these three shells also represent the first set of atoms along [100], [110], and [111], respectively. Outer atoms, which are located within distances $L/2$ along [100], $L/\sqrt{2}$ along [110], and $\sqrt{3}L/2$ along [111] direction, from the vacancy site were found to respond to the presence of a defect and to show some degree of relaxation.

Relaxations of atoms in different shells in defected systems differ in magnitude as well in sign. The atomic displacement field induced by the negatively charged Mg-site vacancy is visualized in Figure 2a. The first shell atoms (i.e., O ions) carrying net negative charges are pushed away from the defect site. However, the second shell atoms (i.e., Mg ions), being positively charged, are pulled toward the defect site and the third shell atoms (i.e., O ions), being negatively charged, are pushed away from the defect site. At zero pressure, the magnitudes of the displacements of the first, second, and third shell atoms from their original positions are 6.46, 4.57, and 0.40%, respectively, of the equilibrium Mg-O bond length (d). Figure 2b shows the atomic displacement field induced by the positively charged O-site vacancy. The first shell atoms (Mg ions) show outward relaxation, the second shell atoms (i.e., O ions) show inward relaxations, and the third shell atoms (i.e., Mg ions) show outward relaxations. At zero pressure, the magnitudes of the relaxations in the first, second, and third shells are, respectively, 8.39%, 3.73%, and 0.64% of d. Most of the atomic relaxations occur in the first and second shells and the relaxation decays rapidly beyond the first three shells.

The effects of pressure on the atomic structure of the defect systems were found to be substantial (Fig. 3). Though the relaxations are generally suppressed with increasing pressure, some cases show some degree of non-monotonic behavior. For both

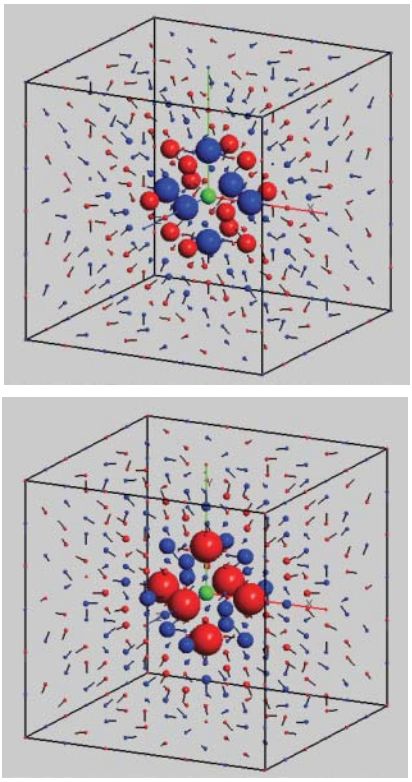

FIGURE 2. Visualization of atomic displacements induced by (**a**) the Mg^{2+} vacancy and (**b**) the O^{2-} vacancy in the 216-site system. The size of the sphere and the orientation of the line, respectively, represent the magnitude and direction of the displacement of a given atom (Mg or O) relative to its position in the perfect crystal. Note that some minimum size was given to each sphere to make it visible on display. The Mg and O atoms are displayed as red and blue spheres, respectively, whereas the vacancy site is shown as a green sphere. In **a** for the Mg^{2+} vacancy, the nearest (N) neighboring atoms (the first shell) are the largest blue spheres, the next-nearest (NN) neighboring atoms (the second shell) are the largest red spheres, the next-next nearest (NNN) neighboring atoms (the third shell) are the second-largest blue spheres, and so on.

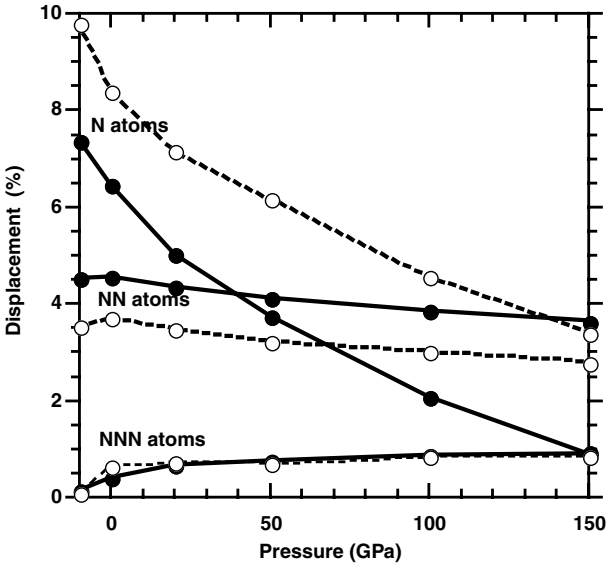

FIGURE 3. Pressure dependence of the atomic displacements in the first, second, and third ionic shells (containing N, NN, and NNN neighboring atoms) for (**a**) the Mg^{2+} vacancy, shown by solid lines, and (**b**) the O^{2-} vacancy, shown by dashed lines.

ionic vacancies, the magnitudes of the relaxations of the first shell (N) atoms decrease relatively much faster than those of the second and third shell atoms. At high pressures (100 GPa or higher), the N atoms in the Mg vacancy system move less than the NN atoms do. A similar crossover in displacement between N and NN atoms can be expected to occur at a much higher pressure (above 150 GPa) in the case of the O vacancy (see Fig. 3).

Electronic structure

In MgO, Mg atoms give up their valence electrons, which along with those from the O atoms are primarily localized in the vicinity of O ions, thereby making the oxide highly ionic in nature. The charges associated with the Mg and O vacancy defects are thus of opposite sign. These charged defects are expected to induce a strong distortion of the valence electron clouds around neighboring ions. The calculated defect-induced electronic structures were explored in detail by visualizing the differences in 3D valence-electron density between defective and perfect systems. However, looking at such differences makes sense only for the unrelaxed systems, which are considered here. In relaxed vacancy systems the charge distribution is also strongly influenced by ionic displacements and it is non-trivial to isolate the contribution arising only from the defect. Visualization considering the density differences for the relaxed systems is currently in progress.

Figures 4a and 4b show the charge density differences (defective-perfect) for both point defects. Two color-mapping scales are used. A fine-level scale uses red and blue to represent the positive and negative differences with magnitudes up to 0.002 (in units of $Å^{-3}$) whereas a coarse-level scale adds a green component to the red and blue colors to map the positive and negative differences with magnitudes higher than 0.002. Thus the black-to-red-to-yellow range maps the regions where electrons are deposited (moved in) and the black-to-blue-to-cyan range maps the regions where electrons are depleted (moved away). Substantial distortions were found to occur in the electron clouds of neighboring ions around each defect. For the Mg vacancy, the valence electrons associated with neighboring O ions are repelled by the negatively charged defect as displayed by blue regions surrounding the O sites and red regions toward Mg sites (Fig. 4a). Nearly the same behavior (with much smaller degree of distortion) is seen around the O sites further away from the defect. We also note that the mostly blue regions surrounding the defect site indicate depletion of electrons. For the positively charged O vacancy, the electrons from the neighboring O ions are pulled toward the defect site; more along [110] directions than along [100] directions. Note that mostly red regions surround the defect site (which is the blue region) in Figure 4b. The oxygen *p* orbitals pointing toward the vacancy are directly involved in the charge redistribution in both cases; the effects are reflected in the blue regions, which are mostly aligned toward the defect site.

The difference valence electron density (defective - perfect)

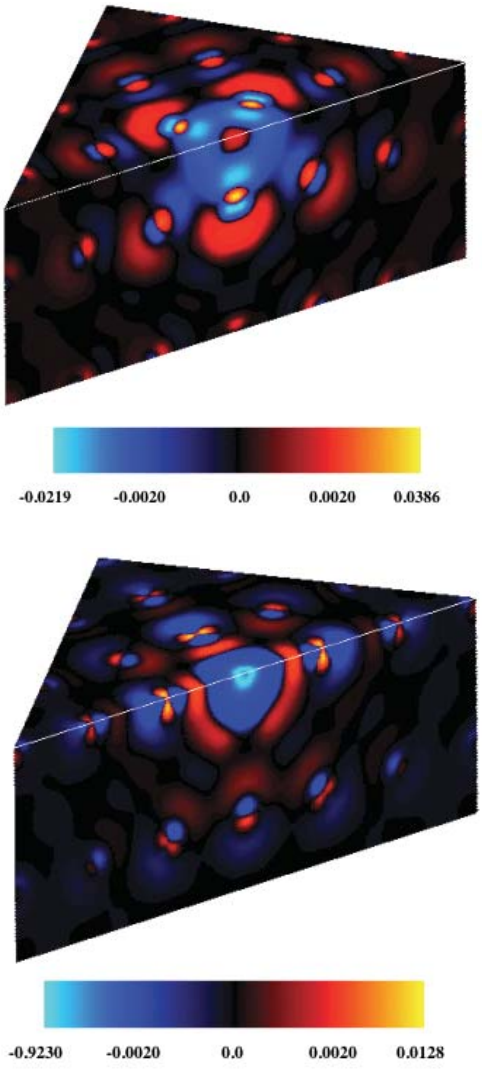

FIGURE 4. Visualization of electron density (in units of Å^{-3}) induced by (**a**) the Mg^{2+} vacancy and (**b**) the O^{2-} vacancy in the 216-site system at zero pressure using planar clipping. Note that the charge density displayed is the difference in the valence electron density between defective and perfect crystals. The volume data is clipped using two planes passing through the vacancy site, which is located at the center of the super cell. Thus, the vertical surface of the clipped super cell represents the (100) plane whereas the vertical surface represents the (110) plane.

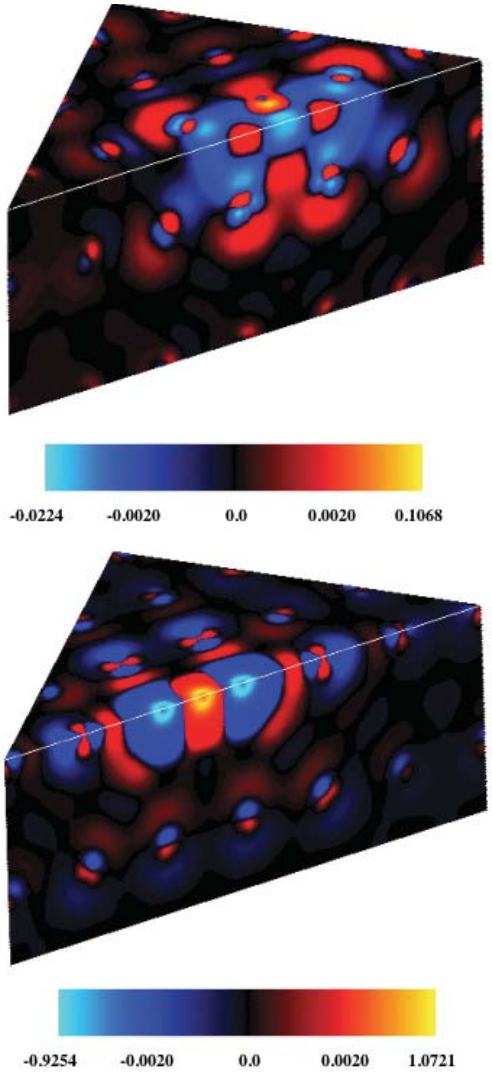

FIGURE 5. Difference valence electron density (in units of Å^{-3}) for (**a**) the migrating Mg^{2+} vacancy and (**b**) the migrating O^{2-} vacancy in the 216-site system, visualized using the same clipping technique as in Figure 4. The horizontal and vertical surfaces, respectively, represent the (100) and (110) planes.

was also visualized for a migrating ion when it is held at the saddle point, midway between initial and final vacancy sites for both Mg and O ions (Figs. 5a and 5b). The electronic structures of the neighboring ions remain essentially unchanged, compared to those for non-migrating defects, as shown in Figures 4a and 4b. The structures in the vicinity of the migrating ion clearly represent the existence of two half-vacancies separated by the ion itself. The defect-induced electronic structures were, in general, found to remain qualitatively unaffected by pressure although the sizes and intensities of the red and blue regions vary to some extent.

IMPLICATIONS FOR RHEOLOGY

Knowledge about defects in major mantle minerals plays an important role in modeling rheological properties of the Earth's mantle as the dominant deformation mechanism in the deep interior is thought to be diffusive in nature. Defect energetics controls diffusion in a mineral to a large extent. For instance, defect concentration is exponentially inversely dependent on defect energy: $n \infty \exp(-\Delta E_f / kT)$ where ΔE_f is the formation energy and n is the number of defects. The diffusion rate can be estimated with knowledge of height and shape of the energy barrier over which a migrating ion must cross, possible diffusion paths, and jump distances: $D \infty \exp(-Q / kT)$, where the activation energy (Q) is the sum of energies of vacancy formation and migration. In MgO, there are 12 equivalent shortest paths for diffusion of both

Mg and O ions. These paths are along [110] and involve jump distance of $a/\sqrt{2}$. Our results show that pressure substantially suppresses both defect concentration and vacancy-mediated diffusion rate because both vacancy formation and migration energies are shown to increase with increasing pressure. However, the temperature is expected to enhance intrinsic defect concentration and diffusion rate (Ita and Cohen 1997). It is also important to note that ionic diffusion in MgO is controlled to large extent by impurities such as Fe^{3+}, Al^{3+}, and Cr^{3+}.

ACKNOWLEDGMENTS

The authors thank J. Brodholt (University College London) for helpful discussions. This work was supported by an NSF Career Grant (EAR 0347204). Computing facilities were provided by the Center of Computation and Technology (CCT) and the Biological Computation and Visualization Center (BCVC) at Louisiana State University.

REFERENCES CITED

Alfe, D. and Gillan, M.J. (2005) The Schottky defect formation energy in MgO calculated by diffusion Monte Carlo. Physical Review B, 71, 220101.

Baroni, S., Giannozzi, P., and Testa, A. (1987) Green's-function approach to linear response in solid. Physical Reviews Letters, 58, 1861–1864.

Brodholt, J.P. (1997) Ab initio calculations on point defects in forsterite (Mg_2SiO_4) and implications for diffusion and creep. American Mineralogist, 82, 1049–1053.

De Vita, A., Gillan, M.J., Lin, J.S., Payne, M.C., Stich, I., and Clarke, L.J. (1992a) Defect energetics in MgO treated by first-principles methods. Physical Review B, 46, 12964–12973.

——— (1992b) Defects in oxide materials from first principles. Physical Review Letters, 68, 3319–3322.

Duclot, M. and Departes, C. (1980) Effect of impurities on cationic conductivity of magnesium-oxide single-crystals. Journal of Solid State Chemistry, 31, 337–385.

Giannozzi, P., de Gironcoli, S., Pavone, P., and Baroni, S. (1991) Ab initio calculations of phonon dispersions in semiconductors. Physical Review B, 43, 7231–7242.

Gibson, A., Haydock, R., and LaFemina, J.P. (1994) Stability of vacancy defects in MgO: the role of charge neutrality. Physical Review B, 50, 2582–2592.

Humphrey, W., Dalke, A., and Schulten, K. (1996) VMD - Visual Molecular Dynamics. Journal of Molecular Graphics, 14, 3–38.

Ita, J. and Cohen, R.E. (1997) Effects of pressure on diffusion and vacancy formation in MgO from non-empirical free-energy integrations. Physical Review Letters, 79, 3198–3200.

——— (1998) Diffusion in MgO at high pressures: Implications for lower mantle rheology. Geophysical Research Letters, 25, 1095–1098.

Karki, B.B., Wentzcovitch, R.M., de Gironcoli, S., and Baroni, S. (2000) High pressure lattice dynamics and thermoelasticity of MgO. Physical Review B, 61, 8793–8800.

Khanduja, G. and Karki, B.B. (2005) Visualization of 3D scientific datasets based on interactive clipping. Proceedings of WSCG International Conference in Central Europe of Computer Graphics, Visualization, and Computer Vision; ISBN 80-903100-9-5. Pages 33–36.

Kokaji, A. (1999) XcrySDen—a new program for displaying crystalline structures and electron densities. Journal of Molecular Graphics Modelling, 17, 176–179.

——— (2003) Computer graphics and graphical user interfaces as tools in simulations of matter at the atomic scale. Computational Materials Science, 28, 155–168.

Lento, J. Mozoz, J.L., and Nieminen, R.M. (2002) Charged point defects in semiconductors and the supercell approximation. Journal of Physics: Condensed Matter, 14, 2637–2645.

Leslie, M. and Gillan, M.J. (9185) The energy and elastic dipole tensor of defects in ionic crystals calculated by the supercell method. Journal of Physics: Condensed Matter, 18, 973–982.

Mackrodt, W.C. (1982) Computer Simulations of Solids. Edited by C.R.A. Catlow and W.C. Mackrodt, pp. 175, Springer-Verlag, Berlin.

Mills, D.R., Parker, S.C., and Wall, W. (1991) The effect of pressure on Schottky pair formation in MgO—a lattice dynamics approach. Philosophical Magazine A, 64, 1133–1144.

Monkhorst, H.J. and Pack, J.D. (1976) Special points for Brillouin-zone integrations. Physical Review B Solid State, 13, 5188–5192.

Mukherjee, S., Cohen, R.E. and Gulseren, O. (2003) Vacancy formation enthalpy at high pressures in tantalum. Journal of Physics: Condensed Matter, 15, 855–861.

Ogut, S. and Chelikowsky, J.R. (2001) Ab initio investigation of point defects in bulk Si and Ge using a cluster method. Physical Review B, 64, 245206.

Sangster, M.J.L. and Rowell, D.K. (1981), Calculation of defect energies and volumes in some oxides. Philosophical Magazine A, 44, 613–624.

Schroeder, W., Martin, K., and Lorensen, B. (1997) Visualization Toolkit: An Object-Oriented Approach to 3D Graphics. Prentice Hall, Upper Saddle River, New Jersey.

Scorza, E., Birkenheuer, U., and Pisani, C. (1997) The oxygen vacancy at the surface and in bulk MgO: an embedded-cluster study. Journal of Chemical Physics, 107, 9645–9658.

Sempolinski, D.R. and Kingery, W.D. (1980) Ionic conductivity and magnesium vacancy mobility in magnesium oxide. Journal of American Ceramics Society, 63, 664–669.

Sharma, A., Haas, A., Nakano, A., Kalia, R., Vashishta, P., Kodiyalam, S., Miller, P., Zhao, W., Liu, X., and Campbell, T.J. (2003) Immersive and interactive exploration of billion-atoms systems. Proceedings of IEEE Virtual Reality Conference, 12, 85–95.

Shirasaki, S. and Hama, M. (1973) Oxygen-diffusion characteristics of loosely sintered polycrystalline MgO. Chemical Physics Letters, 20, 361–365.

Shirasaki, S. and Yamamura, H. (1970) Japanese Journal of Applied Physics, 12, 1634.

Vocaldo, L., Wall, A., Parker, S.C., and Price, G.D. (1995) Absolute ionic diffusion in MgO – computer calculations via lattice dynamics. Physics of Earth and Planetary Interiors, 88, 193 210.

Walker, A.M., Wright, K., and Slater, B. (2003) A computational study of oxygen diffusion in olivine. Physics and Chemistry of Minerals, 30, 536–545.

Watson, G.W., Wall, A., and Parker, S.C. (2000) Atomistic simulation of the effect of temperature and pressure on point defect formation in $MgSiO_3$ perovskite and the stability of $CaSiO_3$. Journal of Physics: Condensed Matter, 12, 8427–8438.

Wright, K and Catlow, C.R.A. (1994) A computer simulation study of (OH) defects in olivine. Physics and Chemistry of Minerals, 20, 515–518.

Wright, K. and Price, G.D. (1993) Computer simulations of defects and diffusion in perovskites. Journal of Geophysical Research, 98, 22245–22253.

Yang, M.H. and Flynn, C.P. (1994) Intrinsic diffusion properties of an oxide: MgO. Physical Review Letters, 73, 1809–1812.

MANUSCRIPT RECEIVED NOVEMBER 19, 2004
MANUSCRIPT ACCEPTED JUNE 3, 2005
MANUSCRIPT HANDLED BY LEE GROAT